ACS OMEGA

Open Access

http://pubs.acs.org/journal/acsodf

Article

Microwave Absorption Performance of Flexible Porous PVDF-MWCNT Foam in the X-Band Frequency Range

Vaishnavi Khade and Madhuri Wuppulluri*

Cite This: *ACS Omega* 2024, 9, 35364−35373

Read Online

ACCESS | Metrics & More | Article Recommendations | Supporting Information

ABSTRACT: Lightweight electromagnetic absorbers made of polymers and multiwall carbon nanotubes (MWCNTs) have attracted a lot of attention because of their potential to shield next-generation electronics devices from electromagnetic radiation without reflecting it back into space. In this research, a flexible foam composed of MWCNTs and polyvinylidene fluoride (PVDF) is developed. This foam is designed to be an electromagnetic shielding material that is both flexible and absorption-dominant, reducing electromagnetic interference. The solvent approach is used to fabricate the PVDF-MWCNT foam. It is discovered that the foam has a porosity of 88.9%. Each cell in the PVDF-MWCNT foam is formed in a porous layered manner. The foam demonstrates a dielectric constant (ϵ') of around 7.19 and dielectric loss (ϵ'') of 4.46 at 9.96 GHz as calculated from MATLAB using the Nicolson−Ross−Wire algorithm. This developed EM absorber exhibits a high shielding efficiency of 78.46 dB. With an ideal reflection loss of −26.5 dB, this absorber attains the desired outcomes. The electromagnetic shielding performance is supported by calculations of the impedance matching degree, which was found to be 0.54. The PVDF-MWCNT foam displayed absorption-dominant characteristics, with a significantly low shielding due to reflection. This newly developed foam EM absorber has proven itself capable in a variety of commercial and stealth-related applications.

INTRODUCTION

In contemporary times, there has been a notable advancement in wireless communication technology and electronic gadgets, encompassing mobile devices, laptops, domestic appliances, medical devices, military radars, and aerospace communications. This progress has significantly contributed to enhancing the convenience and ease of our daily lives.[1] On the other hand, the production of electromagnetic (EM) radiation that is not desirable has a negative impact, which results in the deterioration of the dependability of highly sensitive electronic equipment and has a negative impact on human health.[1,2] Significant endeavors have been undertaken to mitigate the issues arising from electromagnetic interference (EMI) pollution through the development of materials that possess efficient electromagnetic wave attenuation and EMI shielding properties.[3−7]

In order to address these issues, it is of utmost important to focus on the development of EMI shielding materials that possess characteristics such as lightweight composition, high electrical conductivity, resistance to corrosion, and superior performance. In recent years, there has been a significant use of porous carbon materials, particularly carbon foams, across diverse domains. These materials have garnered considerable interest for their application in electromagnetic interference (EMI) shielding. This interest stems from their distinctive three-dimensional open-cell structure, substantial surface area, and exceptional capacity for electromagnetic wave absorption.[8−11] In order to provide effective electromagnetic interference (EMI) shielding and absorption, it is generally necessary to use fillers that possess both dielectric loss and magnetic loss properties. Polymeric porous materials have emerged as the predominant choice for electromagnetic wave absorption in the market due to their robust viscoelastic properties, cost-effectiveness, straightforward manufacturing processes, and convenient integration.[12,13] Poly(vinylidene fluoride) (PVDF) is an extensively studied polymer that is utilized in the preparation of functional foams with diverse applications. This is mostly owing to its exceptional chemical resistance, biocompatibility, thermal and mechanical stability, and UV tolerance capability. Various carbon-based fillers have been employed to attain effective electromagnetic interference (EMI) shielding due to their notable electrical conductivity

Received: January 31, 2024
Revised: May 15, 2024
Accepted: May 16, 2024
Published: August 6, 2024

https://doi.org/10.1021/acsomega.4c00995
ACS Omega 2024, 9, 35364−35373

and substantial surface area.[11,14−16] Also, these possess low weight, corrosion resistance, and high surface area.[17,18,8,19] In the past, numerous scientists have developed various techniques to produce porous carbon materials, including pitch-based and polymer-based carbon foams.[17,20,21] Narasimman et al.[22] have successfully fabricated carbon foam with multiwalled carbon nanotubes (MWCNTs) through the thermoforming technique, utilizing molten sucrose as the precursor material. Their study revealed an impressive electromagnetic interference shielding effectiveness (EMI SE) of up to −39 dB. The polymer-based carbon foams demonstrate economic viability as a result of their capacity for low-temperature heat treatment. However, it should be noted that the properties of these foams are suboptimal, since they exhibit lower conductivity. Consequently, researchers have endeavored to fabricate carbon composite foams by employing various polymers and conductive fillers in order to enhance their electromagnetic interference shielding effectiveness (EMI SE).[11,23] Some reported literatures are tabulated in Table 1. The current investigation involves the fabrication of

Table 1. Some Reported Literature on Carbon Composite Foams[a]

composite foam	EMI SE (dB)	refs
graphene-PDMS	20	11
graphene-PMMA	19	24
PI-Rgo	21	25
PEI-graphene	20	26
sucrose-graphene	38	27
sucrose-MWCNTs	39	28
PU-rGO	20	29
carbon-rGO	44.6	30
graphene-ABS	42.4	31
Mxene-graphene	50.7	32

[a]PMMA, polymethylmethacrylate; PDMS, polydimethylsiloxane; PI, polyimide; PEI. polyetherimide; rGO, reduced graphene oxide; PU, polyurethane; ABS, acrylonitrile butadiene styrene.

PVDF-multiwalled carbon nanotube (MWCNT) hybrid foams by employing a PVDF as a polymer and MWCNTs as a carbon filler. Ultralight weight PVDF foam is synthesized through the utilization of table salt as the sacrificial layer and MWCNTs as a reinforcement. This foam is found to exhibit enhanced electromagnetic interference (EMI) shielding and a hydrophobic nature. The electromagnetic interference (EMI) shielding effectiveness of hybrid foams composed of PVDF and MWCNTs is comprehensively examined within the X-band frequency range (8−12 GHz). The integration of MWCNTs into PVDF foam has significantly enhanced its electromagnetic interference (EMI) shielding capabilities, particularly in terms of absorption and hydrophobic nature while maintaining a low-density characteristic. Furthermore, the PVDF-MWCNTs hybrid foam exhibits open-cell architectures that provide enhanced attenuation of electromagnetic (EM) wave absorption. Hence, the PVDF-MWCNTs hybrid foam is a potential candidate for EMI shielding application in the fields of defense and aerospace.

EXPERIMENTAL PROCEDURE

Synthesis Process for PVDF-MWCNT Foam. The porous ultralight PVDF-MWCNT foam is produced by mixing PVDF pellet (Sigma-Aldrich, USA), table salt (NaCl) (14 g, SD. Fine Chem Ltd., India), and MWCNTs (Ad Nano Technologies) with the mass ratio of mPVDF/mtable salt/mMWCNTs = 1:7:0.1 in *N*,*N*-dimethylformamide (DMF) solvent (10 mL, Sigma-Aldrich, USA) using vigorous magnetic agitation at 60 °C and 150 rpm for 1 h. The prepared mixture is thereafter put in hot air oven for 90 °C for 5 h and then allowed to cool at room temperature, resulting in the formation of a polymer composite sample with a black hue. Subsequently, the composite foam was submerged in hot water, and this procedure was repeated every 2 h for a duration of 1 day. The objective was to fully eliminate salt from the samples and obtain the pure porous PVDF-CNT composite foam. The procedure for synthesizing PVDF-MWCNT composite foam is depicted in Figure 1(a). Figure 1(b) displays an image of the prepared PVDF-MWCNT foam.

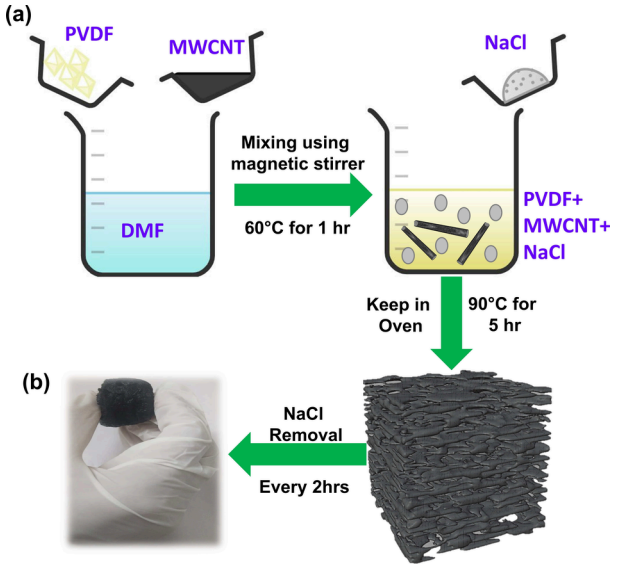

Figure 1. (a) Schematic representation for synthesis of PVDF-MWCNT foam. (b) Image of the PVDF-MWCNT foam.

Characterization and Measurement. The crystal structure is identified using X-ray radiation diffraction (XRD) spectra acquired from a Rigaku Smart Lab diffractometer (Tokyo, Japan) using Cu Kα radiation (λ = 0.15418 nm). The analysis of cellular morphologies is conducted using a JEOL JSM 6060 scanning electron microscope (SEM). Manual image analysis of the SEM images was conducted to assess the average cell size utilizing ImageJ software. The vibrational modes were studied using Fourier transform infrared spectroscopy (FTIR) with a Nicolet iS10 FTIR instrument (USA). The dielectric, impedance, and ac conductivity analysis of the foam were simulated using MATLAB in the 8−12 GHz range. Using a UV−vis spectrometer (JASCO V-670 PC), the bang gap studies were performed for the prepared foam.

In order to test the *S*-parameters in the X-band (8−12 GHz), the PVDF-MWCNT foam is cut into dimensions of 2.3 cm × 1 cm. The vector network analyzer (VNA) method is employed. Using the *S*-parameters, the reflection loss (RL), shielding due to absorption (SE_A), shielding due to reflection (SE_R), and total shielding efficiency (SE_{Total}) are determined. The following equations are used to compute EMI shielding parameters:

$$R = |S_{11}^2| = |S_{22}^2| \quad (1)$$

https://doi.org/10.1021/acsomega.4c00995
ACS Omega 2024, 9, 35364−35373

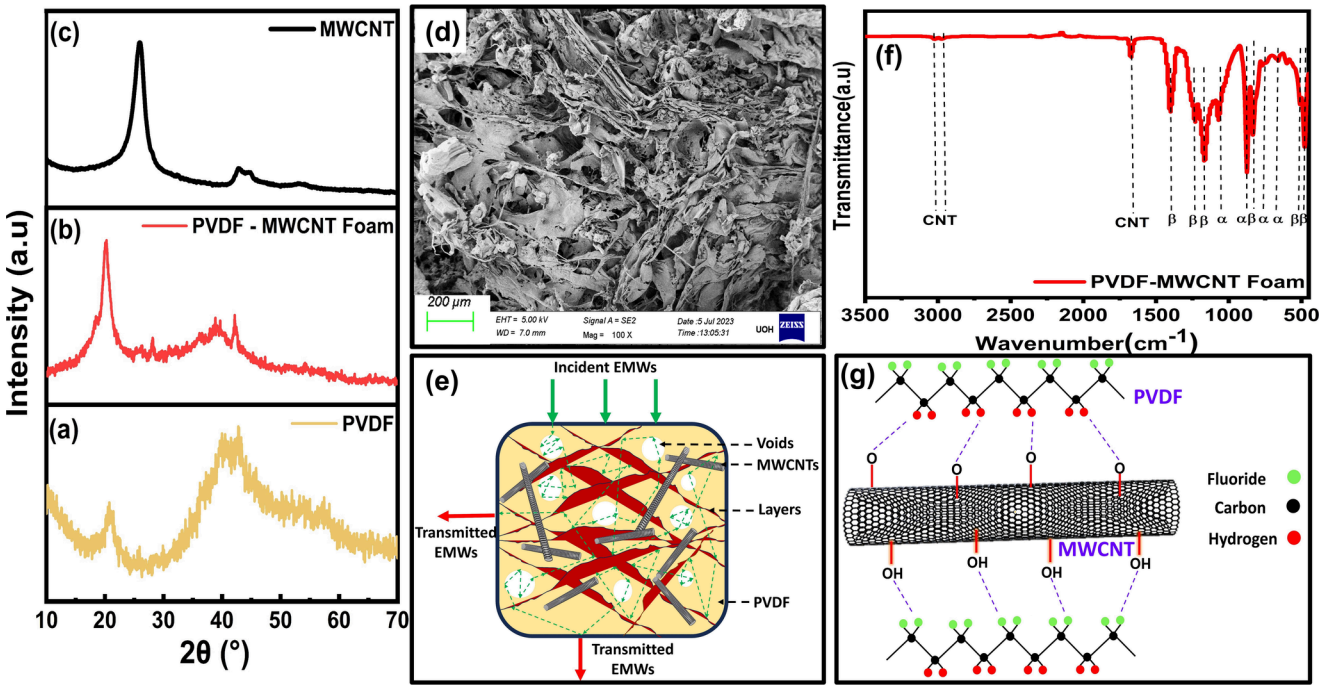

Figure 2. XRD patterns for (a) pure PVDF, (b) PVDF-MWCNT composite, and (c) MWCNT. (d) SEM image of the PVDF-MWCNT composite. (e) EMI shielding mechanism of the flexible foam. (f) FTIR spectra of the PVDF-MWCNT composite foam. (g) Schematic for the interaction of PVDF and MWCNT.

$$T = |S_{12}^2| = |S_{21}^2| \quad (2)$$

$$A = (1 - R - T)/(1 - R) \quad (3)$$

$$\mathrm{RL} = 20\log|S_{11}| \quad (4)$$

$$\mathrm{SE}_A(\mathrm{dB}) = -10\log(1 - A) \quad (5)$$

$$\mathrm{SE}_R(\mathrm{dB}) = 10\log(1/(1 - S_{11}^2)) = 10\log(1/(1 - S_{22}^2)) \quad (6)$$

$$\mathrm{SE}_T(\mathrm{dB}) = 10\log(1/(S_{12}^2)) = 10\log(1/(S_{21}^2)) \quad (7)$$

$$\mathrm{SE}_{\mathrm{Total}} = \mathrm{SE}_A + \mathrm{SE}_R \quad (8)$$

where R, T, and A are reflection, transmission, and absorption coefficients, respectively. Under conditions where the RL is less than 10 dB, the absorption rate of electromagnetic waves (EMWs) is 90% and the reflection rate is 10%. Thus, the effective absorption bandwidth can be termed as the frequency range where RL is less than 10 dB.

RESULTS AND DISCUSSION

X-ray Diffraction Analysis of PVDF-MWCNT Foam. Figure 2(a–c) shows the XRD patterns for PVDF, PVDF-MWNCT foam, and MWCNTs. PVDF and the PVDF-MWNCT foam exhibit distinct peaks at 2θ values of 18.9°, 20.47°, 36.65°, and 39.42° in their XRD patterns. These peaks are attributed to the crystal phases α, β, and γ. The literature states that[33,32] the addition of MWCNTs to a PVDF matrix causes an increase in the β-crystalline phase, which is further explained in detail in the Microstructural Analysis section. Additionally, as can be seen in Figure 2, the 2θ peak at 36.65° (the β-crystalline phase) of the PVDF-MWCNT foam is the most prominent. The β-crystalline polymorph is responsible for the 2θ peaks at 36.46° and 56°, which correspond to Miller indices (101) and (221), respectively. As MWCNTs are introduced to the PVDF matrix, a minor leftward shift of the 2θ peaks is noted.

Microstructural Analysis. The microstructure for PVDF-MWCNT foam is shown in Figure 2(d). The prepared foam is found to have layered structure transformed from the cellular microstructure, which helps for the dissipation of EMWs and multiple internal reflection of these EMWs between the layers of the foam, thus enhancing absorption of EMWs (see Figure 2(e)). Moreover, the sample demonstrated that the polymeric matrix contained high degrees of porosity and interconnectedness of pores across the whole structure. In addition, the SEM images shows that the structures remained almost intact after the inclusion of MWCNTs. Furthermore, the structures of the foam are preserved. The porosity (P) of the porous foam is determined using the following equation:

$$P = V_{\text{PVDF-MWCNT}}/V_{\text{foam}} \quad (9)$$

where V_{PVDF} and V_{MWCNT} represent the actual volumes of the raw materials PVDF and MWCNT, respectively, while V_{foam} represents the overall volume of the foam. The $V_{\text{PVDF-MWCNT}}$ composite may be derived by considering the mass and density of PVDF and MWCNT. On the other hand, the volume of the foam (V_{foam}) can be easily determined based on its size. The porosity the PVDF-MWCNT foam is estimated to be 88.9%.

Fourier Transform-Infrared Spectroscopy (FTIR) Analysis. The synthesized lightweight PVDF-MWCNT foam was analyzed using an FTIR curve within wavenumbers of 400–1500 cm^{-1}. Figure 2(f) illustrates the FTIR spectrum of the sample. The β-phases of the PVDF foam are attributed to the absorption bands that are observed at wavenumbers of 475, 517, 837, 874, 1180, 1218, and 1402 cm^{-1}.[34,35] The presence of an absorption band at a frequency of 515 cm^{-1} indicates the occurrence of a bending vibration in the F–C–F chemical bond.[36] The peaks detected at 832 cm^{-1} corresponded to the

https://doi.org/10.1021/acsomega.4c00995
ACS Omega 2024, 9, 35364–35373

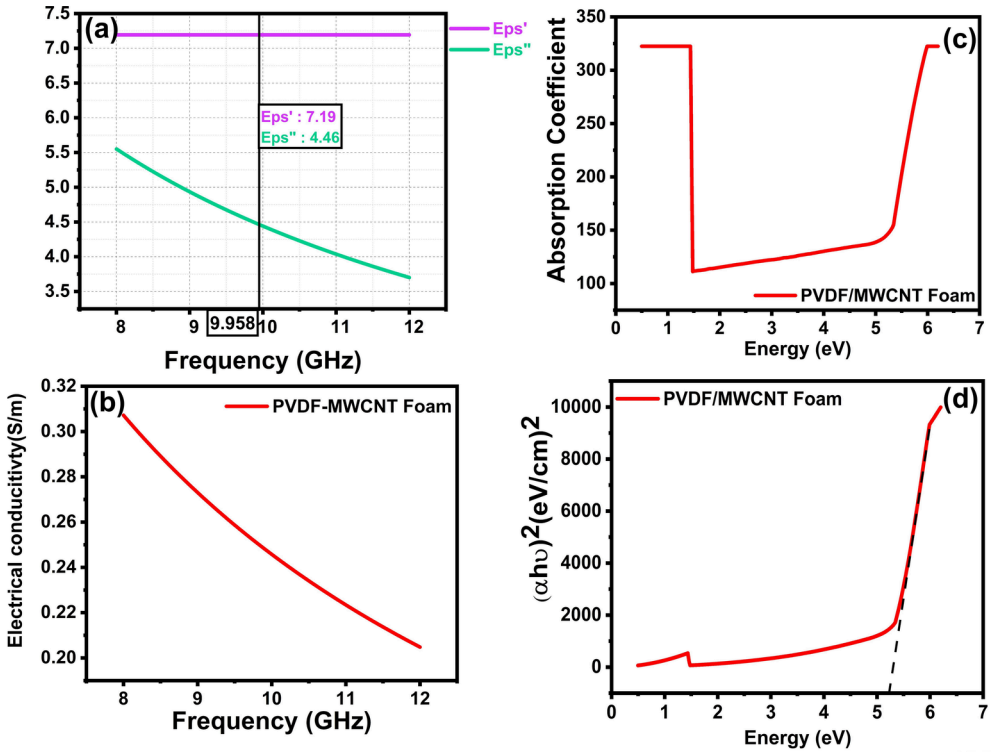

Figure 3. (a) Frequency dependence of ϵ' and ϵ'' of PVDF-MWCNT foam. (b) Frequency-dependent electrical conductivity of PVDF-MWCNT foam. (c) Absorption spectra of the foam. (d) UV−vis spectra of PVDF-MWCNT foam.

rocking motion of the H−C−H bond and the symmetrical stretching of the F−C−F bond, respectively.[37] The absorption bands observed at 1162 cm^{-1} are attributed to the antisymmetric stretching of C−C bonds and the wagging motion of H−C−H bonds. On the other hand, the band discovered at 1228 cm^{-1} is associated with the rocking motion.[38] A peak at 1400 cm^{-1} is attributed to the stretching vibration of the C−F bond in the β-phase of PVDF.[39] Furthermore, a few minor absorbance bands at 614 and 763 cm^{-1} are visible, indicating α- phase. The absorbance bands detected at 1660, 2956, and 3027 cm^{-1} are indicative of carbon nanotubes (MWCNTs) that were incorporated into the PVDF foam. The peak located at 3027 cm^{-1} is indicative of asymmetric CH_2 stretching, whereas the peak at 2956 cm^{-1} is associated with symmetric CH_2 stretching. The absorption peak that is centered at 1660 cm^{-1} is indicative of the carbon skeleton vibrations exhibited by the carbon nanotubes.[40,41] The FTIR analysis also confirmed the presence of β-phase PVDF in the PVDF-MWCNT foam. The transition from the α-phase to the β-phase in the PVDF-MWCNT foam is thought to occur due to the improved compatibility between carboxylic acid groups and CF_2 groups. Additionally, the presence of MWCNTs leads to a strong contact that promotes the crystallization of the β-phase PVDF. In order to verify the proportion of β-phase in the PVDF-MWCNT foam caused by the nucleating agent MWCNT, FTIR analysis of the original PVDF is also conducted under identical conditions (see Figure S1). The fraction of β-phase in both samples is determined using the established equation (provided in the Supporting Information (SI)) based on the analysis of the FTIR spectra. The β-phase contents are determined to be 23.2% and 75.93% for the pure PVDF thin film and PVDF-MWCNT foam, respectively. The outcome demonstrates that MWCNT functions as a polar nucleating agent, inducing the formation of a electroactive phase within the PVDF foam. This may contribute to the EMI shielding efficiency of the foam. In addition, the increased value of the β-phase in the PVDF-MWCNT foam may possibly be attributed to the electrostatic interactions between PVDF and polar molecules, as well as the high viscosity of the polar DMF solvent.[42,43] Figure 2(g) schematically illustrates the interaction between PVDF and MWCNT.

Dielectric Properties. The electromagnetic shielding parameters of an EM absorber have a close relationship with the complex permittivity ($\epsilon_r = \epsilon' + j\epsilon''$) and permeability ($\mu_r = \mu' + j\mu''$) of the absorber. It is important to note that the real components of the complex permittivity (ϵ') and the complex permeability (ϵ') represent the amount of the electric and magnetic energy that can be captured within the material, respectively. Furthermore, the imaginary components, denoted by (ϵ'') and (μ''), are linked to the dissipation energies produced by electromagnetic energy.[44,45] In addition, to this, the EMI shielding efficiency is dependent not only on ϵ'', μ', ϵ'', and μ'' but also the impedance matching.[46,47] Using the Nicolson−Ross−Wire (NRW) algorithm, the complex permittivity (ϵ_r) is extracted[48] in MATLAB. Using NRW, the ϵ_r is calculated using following equation:

$$\epsilon_r \sim \frac{2}{jk_o d}\left(\frac{1 - V_1}{1 + V_1}\right) \tag{10}$$

where $k_o = 2\pi fc$, c is the speed of light, d is thickness, $V_1 = |S_{11}| + |S_{21}|$, in which S_{11} and S_{21} are reflection and transmission coefficients, respectively.[49] Figure 3(a) shows the frequency dependence of ϵ' and ϵ'' simulated by MATLAB in frequency range of 8−12 GHz, and the values are tabulated in Table 2. The dielectric constant is found to be constant over range of frequencies, whereas there is slight decrease in dielectric losses

https://doi.org/10.1021/acsomega.4c00995
ACS Omega 2024, 9, 35364−35373

Table 2. EMI Shielding Parameters for PVDF-MWCNT Foam

parameters	values
ϵ' @ 9.96 GHz	7.19
ϵ'' @ 9.96 GHz	4.46
σ @ 9.96 GHz (S/m)	0.31
S_{11} (dB)	−26.5
S_{12} (dB)	−36.6
SE_A (dB)	71.8
SE_R (dB)	6.65
SE_{Total} (dB)	78.46

with an increase in frequency. In case of dielectric losses, as the applied field frequency increases, the mechanisms of polarization, including space charge, orientation, and ions, fail to keep up with the field and thus the dielectric loss diminishes. The Debye theory is employed to conduct an investigation on the polarization relaxation process. The expression of the correlation between ϵ' and ϵ'' is given below:

$$\left(\epsilon - \frac{\epsilon_s + \epsilon_\infty}{2}\right)'^2 + (\epsilon)''^2 = \left(\frac{\epsilon_s - \epsilon_\infty}{2}\right)^2 \quad (11)$$

where ϵ_s and ϵ_∞ are the static permittivity and the relative dielectric permittivity at the high-frequency limit, respectively. The curve of ϵ' and ϵ'' may be described as a semicircle, known as the Cole−Cole semicircle, which is commonly linked to the phenomenon of Debye polarization relaxation. Due to presence of multiple relaxation, the semicircle displays an arc form. The Figure 4 exhibits the semicircle. The findings of this

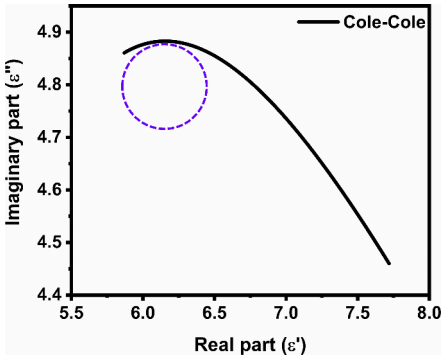

Figure 4. Cole−Cole plot of the PVDF-MWCNT foam.

study confirm the existence of significant interfacial polarization in PVDF-MWCNT foam, which arises from the presence of multiple interfaces. Furthermore, the accumulation of charge carriers occurs at the interface of the sample. This consequently enhances the response to the incoming electromagnetic field, resulting in an increased dielectric polarization loss.[50]

Electrical Conductivity. Based on the free electron theory, the relationship between electrical conductivity (σ) and the frequency (f) of an electromagnetic wave can be expressed as $\epsilon'' = \frac{\sigma}{2\pi\epsilon_0 f}$.[51] A higher electrical conductivity implies higher values of dielectric loss. This equation illustrates the direct correlation between electrical conductivity and the ϵ'' value. Figure 3(b) shows the frequency variation of the electrical conductivity, and the value is tabulated in Table 2. The plot shows a similar trend as the dielectric loss curve. The dielectric loss generally arises from conductivity and polarization losses, encompassing ionic polarization, electronic polarization, dipole orientation polarization, and interfacial polarization. Electron polarization and ion polarization often occur at the THz (terahertz) and PHz (petahertz) scales, respectively. However, for microwave GHz frequencies, the primary contributions to microwave absorption come from dipole orientation polarization and interfacial polarization. The conduction loss is contingent upon the electrical conductivity of the composites, which can be ascertained by evaluating their respective carbon components. In the current case, interfacial polarization dominates because of interfaces between MWNCTs, air, and PVDF. The presence of multiple phases of PVDF in the composite foam led to accumulation of charges, thus contributing to dielectric loss and hence the electrical conductivity of the foam.

UV−vis Spectroscopy Studies. Information on the composition and nature of the material can be gleaned from the optical characteristic of the material. The molecular structure of the material can be determined by monitoring the percentage of absorbance or reflectance. This is possible because of the fact that various molecules absorb different wavelengths of light based on their structures. In addition to assisting in the identification of the bonds that exist between the molecules of the crystal, the data that are received from the spectrometer can also assist in the calculation of the optical characteristics such as the band gap energy.[52−54] The intricacies of the electronic structure of the optical bandgap are provided by the findings that are reported in this research. These studies will help to give proper insight into EMI shielding properties of materials.

A significant change in the band gap can be observed with addition of MWCNT in the PVDF matrix. Figure 3(c) illustrates the absorption spectra of PVDF-MWCNT. It is abundantly clear that the PVDF-MWCNT foam exhibits outstanding transmission across the UV−vis spectrum. In order to have a better understanding of the band structure, it is essential to study the absorption spectrum. The graph Figure 3(d) depicts the relationship between photon energy and $(\alpha h\upsilon)^2$. It is evident that as the photon energy increases, $(\alpha h\upsilon)^2$ also improves. Furthermore, using Tauc's relation (provided in the Supporting Information Supporting Information), the band gap energy is determined by extrapolating the linear region of the plot in Figure 3(d). The difference in energy that exists between the top of the valence band and the bottom of the conduction band of electrons is referred to as the optical bandgap energy (E_g). Thus, direct band gap energy is found to be 5.22 eV.

Electromagnetic Wave Absorption Properties. Vector network analyzer (VNA) is used to experimentally find the electromagnetic interference shielding efficiency (EMI SE). In a two-port VNA, scattering parameters (S_{11} and S_{12}, as well as their reciprocals S_{22} and S_{21}) are used to mathematically express both the incident waves and the transmitted waves. Both the reflection and transmission coefficients are correlated with these S-factors. Thus, reflection (R), transmission (T), and absorption (A) coefficients are calculated using eqs 1 and 2, and the EMI SE of the foam can be expressed using eqs 5−8. Typically, VNA has the ability to actively transmit, receive, and record EM energies across a significantly wider frequency range. Transmission reflection line configurations, which include coaxial cables and waveguide techniques, and free space configurations, such as microwave anechoic chambers,

https://doi.org/10.1021/acsomega.4c00995
ACS Omega 2024, 9, 35364−35373

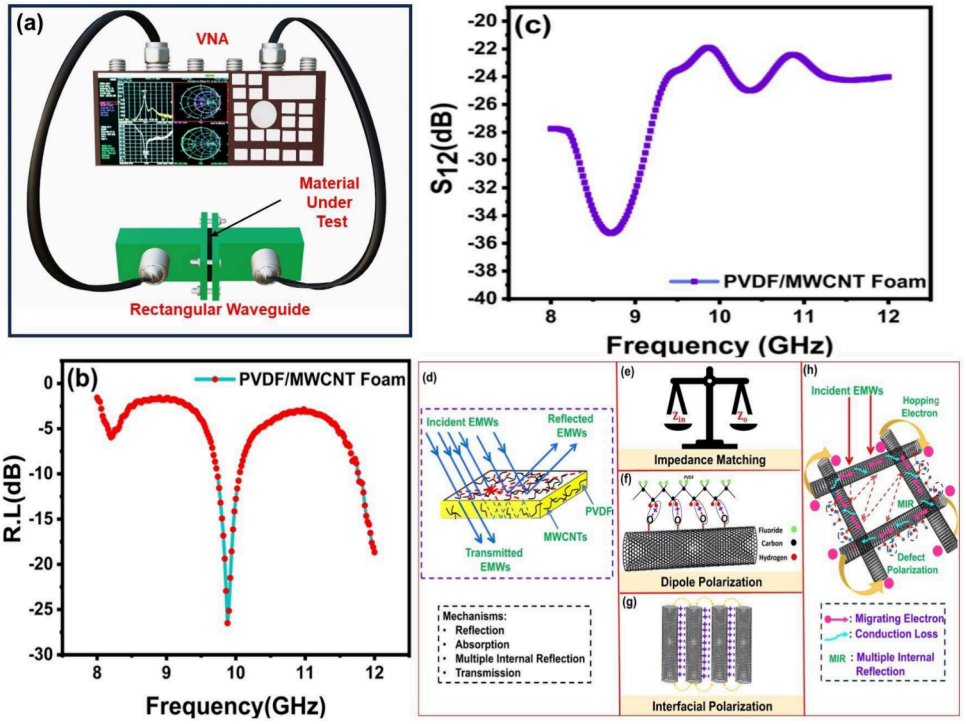

Figure 5. (a) Experimental setup to measure *S*-parameters. (b). Frequency vs RL plot of PVDF-MWCNT foam. (c) Microwave absorption characteristics of the foam (frequency vs S_{12}, (e and f) Phenomena occurring when EMWs interact with the foam.

are the measurement techniques that are most commonly used.[65−67] In current research, we have used the rectangular waveguide transmission line method to measure the EMI SE of the foam. Figure 5(a) shows schematic for this measurement technique. The reflection loss (RL) values of the PVDF-MWCNT foam are calculated at a specified absorber thickness of 0.5 cm in the frequency range of 8−12 GHz. Figure 5(b) shows the variation of RL with frequency. The curve shows the optimal reflection loss of −26.5 dB in the 9−10 GHz frequency bandwidth, indicating that maximum EMWs entering the foam are absorbed and some EMWs are reflected back. This may also be attributed due to the fact that the presence of MWCNTs in a nonconductive PVDF matrix increases the electric conductivity of the foam, thus contributing to shielding due to reflection. Thus, the higher the electrical conductivity, the higher the reflection of EMWs.[68] To further assess the microwave absorption characteristics of the foam S_{12} vs frequency is plotted and analyzed (see Figure 5(c)). It is observed that the foam exhibits a lower transmission loss of −36.57 dB in the 9−12 GHz range, indicating higher microwave absorption. Using the above obtained values, the SE_A, SE_R, and SE_{Total} are estimated, and the values are tabulated in Table 2. It can be concluded from table that shielding due to absorption is the dominant mechanism when EMWs interact with foam. The presence of MWCNTs in the foam provides an additional interface to the foam, thus leading to accumulation of the charges at the interfaces and enhancing interfacial polarization, which in turn contributes to the absorption shielding efficiency of the foam.[69−71] Therefore, due to accumulation of the charges, a charge imbalance will exist between the walls of MWCNTs and PVDF that will lead to significant interfacial loss polarization. In addition, various functional groups of carbon heteroatoms (C−N and C−O) on the MWCNTs can be considered to be dipole active sites. Their symmetry centers differ in some way from the original balance points and as a result they contribute to the intense dipole polarization, which further improves the microwave absorption performance.[72,73]

Along with this, MWCNT foams a stronger interconnected conducting network in the PVDF matrix.I t is imperative to acknowledge that the unique hierarchical tubular configuration plays a pivotal role in enhancing the capacity to attenuate microwaves. The formation of a CNT−CNT in the PVDF matrix reduces the energy barrier associated with electron hopping and provides an extended pathway for the movement of free carriers. The employment of this dual-level conduction network has the potential to significantly enhance the capability for conduction loss, leading to improved dispersion state and thus significantly enhancing EMI shielding performance.[74] Figure 5(d−h) shows phenomenon occurring when EMWs interact with foam. Table 3 shows a comparison of some reported literature based on the EMI shielding efficiency of porous structures.

Table 3. Some Reported Literature on EMI Shielding Effectiveness of Porous Structures in X-Band Frequency

composite foam	EMI SE (dB)	refs
MWCNT-PS	19	55
cellulose-CNTs	21	56
PVDF-MWCNTs	56.7	57
graphene-CNT-PDMS	75	58
robust-CNTs	37.6	59
CNT-GNPs-PMMA	36	60
CNT sponge	54.8	61
CNT-graphene cake	67.4	62
CNTs-MXene-cellulose	38.4	63
carbon-CNTs	57.2	64
PVDF-MWCNT	79.25	present study

https://doi.org/10.1021/acsomega.4c00995
ACS Omega 2024, 9, 35364−35373

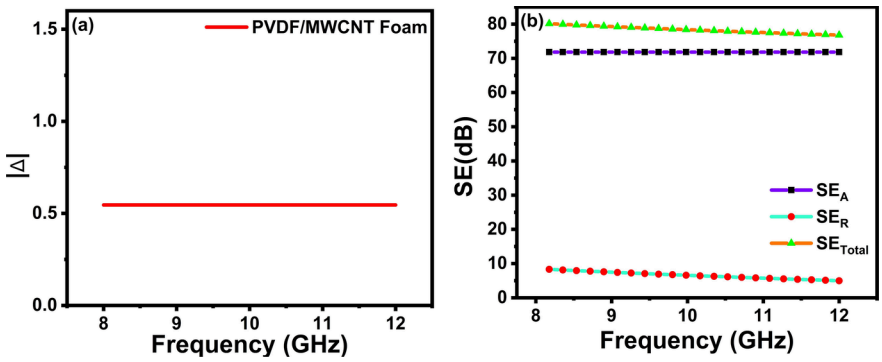

Figure 6. (a) Impedance matching for PVDF-MWCNT foam (8−12 GHz range). (b) Variation of shielding with absorption, reflection, and total shielding of the PVDF-MWCNT foam.

The prime factors contributing to absorption shielding efficiency of any microwave absorbing material are high loss and impedance matching.[75] In order to comprehend the reason for the PVDF-MWCNT foam's superior microwave absorption properties, it is necessary to take into account an additional crucial aspect: impedance matching, which facilitated the transmission of microwaves through the absorbers.[76] In order to total the absorption of electromagnetic waves from surface of the foam, the foam's characteristic impedance should be either equal to or very similar to that of the open space. In order to achieve optimal impedance matching, it is important for the material to possess identical or comparable ϵ' and μ' values. Thus, the impedance matching degree ($\triangle$) is for any material can be calculated using following equation:[77,78]

$$|\triangle| = |\sin h^2(Kfd) - M| \tag{12}$$

$$K = \frac{4\pi\sqrt{\epsilon'\mu'}\sin\frac{\delta_\epsilon + \delta_\mu}{2}}{c\cos\delta_\epsilon\cos\delta_\mu} \tag{13}$$

$$M = \frac{4\pi\epsilon'\mu'\cos\delta_\epsilon\cos\delta_\mu\sqrt{\epsilon'\mu'} \times \sin\frac{\delta_\epsilon + \delta_\mu}{2}}{(\mu'\cos\delta_\epsilon - \epsilon'\cos\delta_\mu) + \tan\left[\frac{\delta_\mu}{2} - \frac{\delta_\epsilon}{2}\right]^2(\mu\cos\delta_\epsilon + \epsilon\cos\delta_\mu)''^2} \tag{14}$$

Note that the lower the impedance matching degree, the better the impedance matching. Figure 6(a) shows the impedance matching for PVDF-MWCNT foam in the 8−12 GHz frequency range. It is observed that the impedance matching degree is constant in the X-band frequency range, and it was found to be 0.54, indicating that the foam is absorption-dominant in the entire X-band frequency range. Thus, the foam has higher microwave absorption performance and impedance matching capabilities.

To further support the absorption-dominant nature of PVDF-MWCNT foam, the SE_A, SE_R, and SE_{Total} values were plotted against the 8−12 GHz range. Figure 6(b) shows the variation of shielding due to the absorption, reflection, and total shielding efficiency in the X-band frequency range. It is clearly evident that the SE_A, SE_R, and SE_{Total} values are almost maintained in the entire X-band frequency range, thus confirming the utility of PVDF-MWCNT foam in the X-band frequency range. Also, it is observed that $SE_A \gg SE_R$, thus indicating the absorption-dominant nature of the X-band frequency range. Hence, PVDF-MWCNT foam is clearly a choice as a electromagnetic absorber in the X-band frequency range.

CONCLUSION

PVDF-MWCNT foam has been developed as EM absorbers through the solution casting method. The foam is found to exhibit porous-layered structure. The FTIR studies suggests that the β-fraction of PVDF increases with the addition of MWCNTs, indicating an electrostatic interaction between PVDF and MWCNTs. Studies of the microwave characteristics as well as the electrical conductivity of the PVDF-MWCNT foam were carried out using the Nicolson−Ross−Wire algorithm through MATLAB in the X-band frequency range. The optical studies show that the foam exhibits an optical band gap of 5.22 eV. Excellent microwave absorbing characteristics are demonstrated by the PVDF-MWCNT foam with thickness of 0.5 cm with an optimal reflection loss of −26.5 dB and S_{12} value of −36.6 dB in 8−12 GHz frequency range. Furthermore, the impedance matching degree is estimated in order to support the enhanced microwave absorbing characteristics of the foam. Therefore, we can conclude that PVDF-MWCNT foam is a potential microwave absorber because it has outstanding properties such as high EMI SE in the X-band frequency range as well as a low thickness and lightweight nature.

ASSOCIATED CONTENT

Supporting Information

The Supporting Information is available free of charge at https://pubs.acs.org/doi/10.1021/acsomega.4c00995.

FTIR analysis for pure PVDF and formula for calculating the β-phase fraction for polymer-based composition and bang gap studies (PDF)

AUTHOR INFORMATION

Corresponding Author

Madhuri Wuppulluri − *Center for Functional Materials and School of Advanced Sciences, Vellore Institute of Technology, Vellore, Tamil Nadu 632014, India;* orcid.org/0000-0002-1650-9931; Email: madhuriw12@hotmail.com

Author

Vaishnavi Khade − *Center for Functional Materials and School of Advanced Sciences, Vellore Institute of Technology, Vellore, Tamil Nadu 632014, India*

Complete contact information is available at: https://pubs.acs.org/10.1021/acsomega.4c00995

https://doi.org/10.1021/acsomega.4c00995
ACS Omega 2024, 9, 35364−35373

Author Contributions

V.K.: Synthesis, data collection, data curing, draft preparation. W.M.: conceptualization, methodology, final drafting, and project supervision.

Notes

The authors declare no competing financial interest.

■ ACKNOWLEDGMENTS

The authors would like to thank SAS, VIT University, for XRD, UV−vis, and FTIR facilities. Thanks to Hyderab Central University for FESEM facilities.

■ REFERENCES

(1) Khade, V.; Wuppulluri, M.; Chandrasekhar, A.; Babu, T. A. Flexible ceramics for EMI shielding applications. In *Advanced Ceramic Coatings*; Gupta, R. K.; Motallebzadeh, A.; Kakooei, S.; Nguyen, T. A.; Behera, A., Eds.; Elsevier, 2023; pp 381−400.

(2) Mariappan, P. M.; Raghavan, D. R.; Aleem, S. H. A.; Zobaa, A. F. Effects of electromagnetic interference on the functional usage of medical equipment by 2G/3G/4G cellular phones: A review. *J. Adv. Res.* **2016**, *7*, 727−738.

(3) Xu, H.; Yin, X.; Li, X.; Li, M.; Liang, S.; Zhang, L.; Cheng, L. Lightweight Ti2CT x MXene/poly (vinyl alcohol) composite foams for electromagnetic wave shielding with absorption-dominated feature. *ACS Appl. Mater. Interfaces* **2019**, *11*, 10198−10207.

(4) Cao, M.-S.; Wang, X.-X.; Zhang, M.; Shu, J.-C.; Cao, W.-Q.; Yang, H.-J.; Fang, X.-Y.; Yuan, J. Electromagnetic response and energy conversion for functions and devices in low-dimensional materials. *Adv. Funct. Mater.* **2019**, *29*, 1807398.

(5) Zhang, W.; Zhao, B.; Xiang, H.; Dai, F.-Z.; Wu, S.; Zhou, Y. One-step synthesis and electromagnetic absorption properties of high entropy rare earth hexaborides (HE REB 6) and high entropy rare earth hexaborides/borates (HE REB 6/HE REBO 3) composite powders. *Journal of Advanced Ceramics* **2021**, *10*, 62−77.

(6) Du, B.; Cai, M.; Wang, X.; Qian, J.; He, C.; Shui, A. Enhanced electromagnetic wave absorption property of binary ZnO/NiCo 2 O 4 composites. *Journal of Advanced Ceramics* **2021**, *10*, 832−842.

(7) Ye, X.; Chen, Z.; Ai, S.; Hou, B.; Zhang, J.; Liang, X.; Zhou, Q.; Liu, H.; Cui, S. Porous SiC/melamine-derived carbon foam frameworks with excellent electromagnetic wave absorbing capacity. *Journal of Advanced Ceramics* **2019**, *8*, 479−488.

(8) Yuan, Y.; Ding, Y.; Wang, C.; Xu, F.; Lin, Z.; Qin, Y.; Li, Y.; Yang, M.; He, X.; Peng, Q.; et al. Multifunctional stiff carbon foam derived from bread. *ACS Appl. Mater. Interfaces* **2016**, *8*, 16852−16861.

(9) Kumar, R.; Dhakate, S. R.; Gupta, T.; Saini, P.; Singh, B. P.; Mathur, R. B. Effective improvement of the properties of light weight carbon foam by decoration with multi-wall carbon nanotubes. *Journal of Materials Chemistry A* **2013**, *1*, 5727−5735.

(10) Li, Q.; Chen, L.; Ding, J.; Zhang, J.; Li, X.; Zheng, K.; Zhang, X.; Tian, X. Open-cell phenolic carbon foam and electromagnetic interference shielding properties. *Carbon* **2016**, *104*, 90−105.

(11) Chen, Z.; Xu, C.; Ma, C.; Ren, W.; Cheng, H.-M. Lightweight and flexible graphene foam composites for high-performance electromagnetic interference shielding. *Advanced materials* **2013**, *25*, 1296−1300.

(12) Chen, L.; Rende, D.; Schadler, L. S.; Ozisik, R. Polymer nanocomposite foams. *Journal of Materials Chemistry A* **2013**, *1*, 3837−3850.

(13) Liu, P.; Chen, G.-F. *Porous materials: Processing and applications*; Elsevier, 2014.

(14) Yang, Y.; Gupta, M. C.; Dudley, K. L.; Lawrence, R. W. Conductive carbon nanofiber−polymer foam structures. *Advanced materials* **2005**, *17*, 1999−2003.

(15) Li, Y.; Liu, J.; Wang, S.; Zhang, L.; Shen, B. Self-templating graphene network composites by flame carbonization for excellent electromagnetic interference shielding. *Composites Part B: Engineering* **2020**, *182*, 107615.

(16) Chaudhary, A.; Kumari, S.; Kumar, R.; Teotia, S.; Singh, B. P.; Singh, A. P.; Dhawan, S.; Dhakate, S. R. Lightweight and easily foldable MCMB-MWCNTs composite paper with exceptional electromagnetic interference shielding. *ACS Appl. Mater. Interfaces* **2016**, *8*, 10600−10608.

(17) Yuan, Y.; Liu, L.; Yang, M.; Zhang, T.; Xu, F.; Lin, Z.; Ding, Y.; Wang, C.; Li, J.; Yin, W.; et al. Lightweight, thermally insulating and stiff carbon honeycomb-induced graphene composite foams with a horizontal laminated structure for electromagnetic interference shielding. *Carbon* **2017**, *123*, 223−232.

(18) Ajitha, A.; Surendran, A.; Aswathi, M.; Geethamma, V.; Thomas, S. Advanced Carbon Based Foam Materials for EMI Shielding. *Advanced Materials for Electromagnetic Shielding: Fundamentals, Properties, and Applications* **2018**, 305−325.

(19) Yang, J.; Liao, X.; Li, J.; He, G.; Zhang, Y.; Tang, W.; Wang, G.; Li, G. Light-weight and flexible silicone rubber/MWCNTs/Fe3O4 nanocomposite foams for efficient electromagnetic interference shielding and microwave absorption. *Compos. Sci. Technol.* **2019**, *181*, 107670.

(20) Chen, C.; Kennel, E. B.; Stiller, A. H.; Stansberry, P. G.; Zondlo, J. W. Carbon foam derived from various precursors. *Carbon* **2006**, *44*, 1535−1543.

(21) Zhang, L.; Liu, M.; Roy, S.; Chu, E. K.; See, K. Y.; Hu, X. Phthalonitrile-based carbon foam with high specific mechanical strength and superior electromagnetic interference shielding performance. *ACS Appl. Mater. Interfaces* **2016**, *8*, 7422−7430.

(22) Narasimman, R.; Prabhakaran, K. Preparation of low density carbon foams by foaming molten sucrose using an aluminium nitrate blowing agent. *Carbon* **2012**, *50*, 1999−2009.

(23) Dhakate, S. R.; Subhedar, K. M.; Singh, B. P. Polymer nanocomposite foam filled with carbon nanomaterials as an efficient electromagnetic interference shielding material. *Rsc Advances* **2015**, *5*, 43036−43057.

(24) Zhang, H.-B.; Yan, Q.; Zheng, W.-G.; He, Z.; Yu, Z.-Z. Tough graphene- polymer microcellular foams for electromagnetic interference shielding. *ACS Appl. Mater. Interfaces* **2011**, *3*, 918−924.

(25) Li, Y.; Pei, X.; Shen, B.; Zhai, W.; Zhang, L.; Zheng, W. Polyimide/graphene composite foam sheets with ultrahigh thermostability for electromagnetic interference shielding. *Rsc Advances* **2015**, *5*, 24342−24351.

(26) Ling, J.; Zhai, W.; Feng, W.; Shen, B.; Zhang, J.; Zheng, W. G. Facile preparation of lightweight microcellular polyetherimide/graphene composite foams for electromagnetic interference shielding. *ACS Appl. Mater. Interfaces* **2013**, *5*, 2677−2684.

(27) Narasimman, R.; Vijayan, S.; Prabhakaran, K. Graphene-reinforced carbon composite foams with improved strength and EMI shielding from sucrose and graphene oxide. *J. Mater. Sci.* **2015**, *50*, 8018−8028.

(28) Narasimman, R.; Vijayan, S.; Dijith, K.; Surendran, K.; Prabhakaran, K. Carbon composite foams with improved strength and electromagnetic absorption from sucrose and multi-walled carbon nanotube. *Mater. Chem. Phys.* **2016**, *181*, 538−548.

(29) Gavgani, J. N.; Adelnia, H.; Zaarei, D.; Gudarzi, M. M. Lightweight flexible polyurethane/reduced ultralarge graphene oxide composite foams for electromagnetic interference shielding. *RSC Adv.* **2016**, *6*, 27517−27527.

(30) Agrawal, P. R.; Kumar, R.; Teotia, S.; Kumari, S.; Mondal, D.; Dhakate, S. R. Lightweight, high electrical and thermal conducting carbon-rGO composites foam for superior electromagnetic interference shielding. *Composites Part B: Engineering* **2019**, *160*, 131−139.

(31) Wang, L.; Wu, Y.; Wang, Y.; Li, H.; Jiang, N.; Niu, K. Laterally compressed graphene foam/acrylonitrile butadiene styrene composites for electromagnetic interference shielding. *Composites Part A: Applied Science and Manufacturing* **2020**, *133*, 105887.

(32) Fan, Z.; Wang, D.; Yuan, Y.; Wang, Y.; Cheng, Z.; Liu, Y.; Xie, Z. A lightweight and conductive MXene/graphene hybrid foam for

https://doi.org/10.1021/acsomega.4c00995
ACS Omega 2024, 9, 35364−35373

superior electromagnetic interference shielding. *Chemical Engineering Journal* **2020**, *381*, 122696.
(33) Mishra, S.; Kumaran, K.; Sivakumaran, R.; Pandian, S. P.; Kundu, S. Synthesis of PVDF/CNT and their functionalized composites for studying their electrical properties to analyze their applicability in actuation & sensing. *Colloids Surf., A* **2016**, *509*, 684−696.
(34) Kabir, E.; Khatun, M.; Nasrin, L.; Raihan, M. J.; Rahman, M. Pure β-phase formation in polyvinylidene fluoride (PVDF)-carbon nanotube composites. *J. Phys. D: Appl. Phys.* **2017**, *50*, 163002.
(35) Chen, F.; Lu, Y.; Liu, X.; Song, J.; He, G.; Tiwari, M. K.; Carmalt, C. J.; Parkin, I. P. Table salt as a template to prepare reusable porous PVDF−MWCNT foam for separation of immiscible oils/organic solvents and corrosive aqueous solutions. *Adv. Funct. Mater.* **2017**, *27*, 1702926.
(36) Kobayashi, M.; Tashiro, K.; Tadokoro, H. Molecular vibrations of three crystal forms of poly (vinylidene fluoride). *Macromolecules* **1975**, *8*, 158−171.
(37) Zhou, R.; Liu, W.; Yao, X.; Leong, Y. W.; Lu, X. Poly (vinylidene fluoride) nanofibrous mats with covalently attached SiO 2 nanoparticles as an ionic liquid host: enhanced ion transport for electrochromic devices and lithium-ion batteries. *Journal of Materials Chemistry A* **2015**, *3*, 16040−16049.
(38) Inamuddin; Abbas Kashmery, H. Polyvinylidene fluoride/sulfonated graphene oxide blend membrane coated with polypyrrole/platinum electrode for ionic polymer metal composite actuator applications. *Sci. Rep.* **2019**, *9*, 9877.
(39) Zhang, Y.; Yang, B.; Li, K.; Hou, D.; Zhao, C.; Wang, J. Electrospun porous poly (tetrafluoroethylene-co-hexafluoropropylene-co-vinylidene fluoride) membranes for membrane distillation. *RSC Adv.* **2017**, *7*, 56183−56193.
(40) Mwafy, E. A.; Dawy, M.; Abouelsayed, A.; Elsabbagh, I.; Elfass, M. Synthesis and Characterization of Multi-Walled Carbon Nanotubes Decorated ZnO Nanocomposite. *Egypt. J. Chem.* **2016**, *59*, 1061−1068.
(41) Kumar N.B, R.; Crasta, V.; Praveen, B.; Kumar, M. Studies on structural, optical and mechanical properties of MWCNTs and ZnO nanoparticles doped PVA nanocomposites. *Nanotechnol. Rev.* **2015**, *4*, 457−467.
(42) Yang, L.; Cheng, M.; Lyu, W.; Shen, M.; Qiu, J.; Ji, H.; Zhao, Q. Tunable piezoelectric performance of flexible PVDF based nanocomposites from MWCNTs/graphene/MnO2 three-dimensional architectures under low poling electric fields. *Composites Part A: Applied Science and Manufacturing* **2018**, *107*, 536−544.
(43) Fortunato, M.; Cavallini, D.; De Bellis, G.; Marra, F.; Tamburrano, A.; Sarto, F.; Sarto, M. S. Phase inversion in PVDF films with enhanced piezoresponse through spin-coating and quenching. *Polymers* **2019**, *11*, 1096.
(44) Han, M.; Yin, X.; Kong, L.; Li, M.; Duan, W.; Zhang, L.; Cheng, L. Graphene-wrapped ZnO hollow spheres with enhanced electromagnetic wave absorption properties. *Journal of Materials Chemistry A* **2014**, *2*, 16403−16409.
(45) Li, H.; Huang, Y.; Sun, G.; Yan, X.; Yang, Y.; Wang, J.; Zhang, Y. Directed growth and microwave absorption property of crossed ZnO netlike micro-/nanostructures. *J. Phys. Chem. C* **2010**, *114*, 10088−10091.
(46) Zhang, X.; Ji, G.; Liu, W.; Quan, B.; Liang, X.; Shang, C.; Cheng, Y.; Du, Y. Thermal conversion of an Fe 3 O 4@ metal−organic framework: a new method for an efficient Fe−Co/nanoporous carbon microwave absorbing material. *Nanoscale* **2015**, *7*, 12932−12942.
(47) Che, R. C.; Peng, L.-M.; Duan, X. F.; Chen, Q.; Liang, X. L. Microwave absorption enhancement and complex permittivity and permeability of Fe encapsulated within carbon nanotubes. *Adv. Mater.* **2004**, *16*, 401−405.
(48) Nicolson, A.; Ross, G. Measurement of the intrinsic properties of materials by time-domain techniques. *IEEE Transactions on instrumentation and measurement* **1970**, *19*, 377−382.
(49) Rahman, M. A.; Islam, M. T.; Singh, M. S. J.; Samsuzzaman, M.; Chowdhury, M. E. Synthesis and characterization of Mg−Zn ferrite based flexible microwave composites and its application as SNG metamaterial. *Sci. Rep.* **2021**, *11*, 7654.
(50) Zhao, B.; Yan, Z.; Du, Y.; Rao, L.; Chen, G.; Wu, Y.; Yang, L.; Zhang, J.; Wu, L.; Zhang, D. W.; et al. High-entropy enhanced microwave attenuation in titanate perovskites. *Adv. Mater.* **2023**, *35*, 2210243.
(51) Shukla, V. Review of electromagnetic interference shielding materials fabricated by iron ingredients. *Nanoscale Advances* **2019**, *1*, 1640−1671.
(52) Seminara, L.; Capurro, M.; Cirillo, P.; Cannata, G.; Valle, M. Electromechanical characterization of piezoelectric PVDF polymer films for tactile sensors in robotics applications. *Sensors and Actuators A: Physical* **2011**, *169*, 49−58.
(53) Yang, Y.; Chan, H. L.; Choy, C. Properties of triglycine sulfate/poly (vinylidene fluoride-trifluoroethylene) 0−3 composites. *J. Mater. Sci.* **2006**, *41*, 251−258.
(54) Batra, A.; Corda, J.; Guggilla, P.; Aggarwal, M.; Edwards, M. Electrical properties of silver nanoparticles reinforced LiTaO3: P (VDF-TrFE) composite films. *Proc. SPIE* **2009**, *7419*, 741904.
(55) Yang, Y.; Gupta, M. C.; Dudley, K. L.; Lawrence, R. W. Novel carbon nanotube- polystyrene foam composites for electromagnetic interference shielding. *Nano Lett.* **2005**, *5*, 2131−2134.
(56) Huang, H.-D.; Liu, C.-Y.; Zhou, D.; Jiang, X.; Zhong, G.-J.; Yan, D.-X.; Li, Z.-M. Cellulose composite aerogel for highly efficient electromagnetic interference shielding. *Journal of Materials Chemistry A* **2015**, *3*, 4983−4991.
(57) Wang, H.; Zheng, K.; Zhang, X.; Ding, X.; Zhang, Z.; Bao, C.; Guo, L.; Chen, L.; Tian, X. 3D network porous polymeric composites with outstanding electromagnetic interference shielding. *Compos. Sci. Technol.* **2016**, *125*, 22−29.
(58) Sun, X.; Liu, X.; Shen, X.; Wu, Y.; Wang, Z.; Kim, J.-K. Graphene foam/carbon nanotube/poly (dimethyl siloxane) composites for exceptional microwave shielding. *Composites Part A: Applied Science and Manufacturing* **2016**, *85*, 199−206.
(59) Li, M.-Z.; Jia, L.-C.; Zhang, X.-P.; Yan, D.-X.; Zhang, Q.-C.; Li, Z.-M. Robust carbon nanotube foam for efficient electromagnetic interference shielding and microwave absorption. *J. Colloid Interface Sci.* **2018**, *530*, 113−119.
(60) Zhang, H.; Zhang, G.; Tang, M.; Zhou, L.; Li, J.; Fan, X.; Shi, X.; Qin, J. Synergistic effect of carbon nanotube and graphene nanoplates on the mechanical, electrical and electromagnetic interference shielding properties of polymer composites and polymer composite foams. *Chemical Engineering Journal* **2018**, *353*, 381−393.
(61) Lu, D.; Mo, Z.; Liang, B.; Yang, L.; He, Z.; Zhu, H.; Tang, Z.; Gui, X. Flexible, lightweight carbon nanotube sponges and composites for high-performance electromagnetic interference shielding. *Carbon* **2018**, *133*, 457−463.
(62) Zhu, S.; Xing, C.; Wu, F.; Zuo, X.; Zhang, Y.; Yu, C.; Chen, M.; Li, W.; Li, Q.; Liu, L. Cake-like flexible carbon nanotubes/graphene composite prepared via a facile method for high-performance electromagnetic interference shielding. *Carbon* **2019**, *145*, 259−265.
(63) Cao, W.; Ma, C.; Tan, S.; Ma, M.; Wan, P.; Chen, F. Ultrathin and flexible CNTs/MXene/cellulose nanofibrils composite paper for electromagnetic interference shielding. *Nano-Micro Letters* **2019**, *11*, 72.
(64) Patle, V. K.; Kumar, R.; Sharma, A.; Dwivedi, N.; Muchhala, D.; Chaudhary, A.; Mehta, Y.; Mondal, D.; Srivastava, A. Three dimension phenolic resin derived carbon-CNTs hybrid foam for fire retardant and effective electromagnetic interference shielding. *Composites Part C: Open Access* **2020**, *2*, 100020.
(65) Lv, H.; Guo, Y.; Yang, Z.; Cheng, Y.; Wang, L. P.; Zhang, B.; Zhao, Y.; Xu, Z. J.; Ji, G. A brief introduction to the fabrication and synthesis of graphene based composites for the realization of electromagnetic absorbing materials. *Journal of Materials Chemistry C* **2017**, *5*, 491−512.

https://doi.org/10.1021/acsomega.4c00995
ACS Omega 2024, 9, 35364−35373

(66) Wang, Y.; Zhao, W.; Tan, L.; Li, Y.; Qin, L.; Li, S. Review of Polymer-Based Composites for Electromagnetic Shielding Application. *Molecules* **2023**, *28*, 5628.
(67) Qin, F.; Peng, H.; Pankratov, N.; Phan, M.; Panina, L.; Ipatov, M.; Zhukova, V.; Zhukov, A.; Gonzalez, J. Exceptional electromagnetic interference shielding properties of ferromagnetic microwires enabled polymer composites. *J. Appl. Phys.* **2010**, *108*, 044510.
(68) Zhao, B.; Hamidinejad, M.; Wang, S.; Bai, P.; Che, R.; Zhang, R.; Park, C. B. Advances in electromagnetic shielding properties of composite foams. *Journal of Materials Chemistry A* **2021**, *9*, 8896−8949.
(69) Zhang, D.; Liu, T.; Cheng, J.; Cao, Q.; Zheng, G.; Liang, S.; Wang, H.; Cao, M.-S. Lightweight and high-performance microwave absorber based on 2D WS 2−RGO heterostructures. *Nano-Micro letters* **2019**, *11*, 38.
(70) Sani, Y.; Azis, R. S.; Ismail, I.; Yaakob, Y.; Mohammed, J. others Enhanced electromagnetic microwave absorbing performance of carbon nanostructures for RAMs: A review. *Appl. Surf. Sci. Adv.* **2023**, *18*, 100455.
(71) Khade, V.; Thirumalasetty, A. B.; Rathod, A. A.; Chaoukiker, Y. K.; Wuppulluri, M. Flexible and rigid spinel ferrite carboneous composite as a future of tunable absorption dominant cmWave shielding materials. *J. Mater. Chem. A* **2024**, *12*, 8914.
(72) Sun, H.; Che, R.; You, X.; Jiang, Y.; Yang, Z.; Deng, J.; Qiu, L.; Peng, H. Cross-stacking aligned carbon-nanotube films to tune microwave absorption frequencies and increase absorption intensities. *Advanced materials* **2014**, *26*, 8120−8125.
(73) Wu, Z.; Pei, K.; Xing, L.; Yu, X.; You, W.; Che, R. Enhanced microwave absorption performance from magnetic coupling of magnetic nanoparticles suspended within hierarchically tubular composite. *Adv. Funct. Mater.* **2019**, *29*, 1901448.
(74) Shayesteh Zeraati, A.; Mende Anjaneyalu, A.; Pawar, S. P.; Abouelmagd, A.; Sundararaj, U. Effect of secondary filler properties and geometry on the electrical, dielectric, and electromagnetic interference shielding properties of carbon nanotubes/polyvinylidene fluoride nanocomposites. *Polym. Eng. Sci.* **2021**, *61*, 959−970.
(75) Qiao, M.; Lei, X.; Ma, Y.; Tian, L.; He, X.; Su, K.; Zhang, Q. Application of yolk−shell Fe 3 O 4@ N-doped carbon nanochains as highly effective microwave-absorption material. *Nano Research* **2018**, *11*, 1500−1519.
(76) Liu, W.; Shao, Q.; Ji, G.; Liang, X.; Cheng, Y.; Quan, B.; Du, Y. Metal−organic-frameworks derived porous carbon-wrapped Ni composites with optimized impedance matching as excellent lightweight electromagnetic wave absorber. *Chemical Engineering Journal* **2017**, *313*, 734−744.
(77) Guo, J.; Song, H.; Liu, H.; Luo, C.; Ren, Y.; Ding, T.; Khan, M. A.; Young, D. P.; Liu, X.; Zhang, X.; et al. Polypyrrole-interface-functionalized nano-magnetite epoxy nanocomposites as electromagnetic wave absorbers with enhanced flame retardancy. *J. Mater. Chem. C* **2017**, *5*, 5334−5344.
(78) Zhao, B.; Guo, X.; Zhao, W.; Deng, J.; Fan, B.; Shao, G.; Bai, Z.; Zhang, R. Facile synthesis of yolk−shell Ni@ void@ SnO 2 (Ni 3 Sn 2) ternary composites via galvanic replacement/Kirkendall effect and their enhanced microwave absorption properties. *Nano Research* **2017**, *10*, 331−343.

https://doi.org/10.1021/acsomega.4c00995
ACS Omega 2024, 9, 35364−35373